Applied Catalysis B: Environmental 132–133 (2013) 219–228

Contents lists available at SciVerse ScienceDirect

Applied Catalysis B: Environmental

journal homepage: www.elsevier.com/locate/apcatb

A salt-assisted approach for the pore-size-tailoring of the ionic-liquid-templated TiO_2 photocatalysts exhibiting high activity

Sue-min Chang*, Chung-yu Lee

Institute of Environmental Engineering, National Chiao Tung University, 1001, University Road, Hsinchu 30010, Taiwan

ARTICLE INFO

Article history:
Received 2 September 2012
Received in revised form 28 October 2012
Accepted 11 November 2012
Available online 7 December 2012

Keywords:
Ionic liquids
Salt-assisting
Mesoporous materials
Pore expansion
Photocatalysis

ABSTRACT

In this study, we develop a novel salt-assisted approach to adjusting the pore size of ionic-liquid-templated TiO_2 photocatalysts by simply changing the concentrations and types of the inorganic salts. Four types of salts, including NaCl, $CaCl_2$, NH_4Cl, and NH_4NO_3, are selected in order to investigate the effects of the ionic radii and the charges of the constituent ions on the resulting textures. In addition, a mechanism that the salts assist the self-assembly of hydrophilic 1-butyl-3-methylimidazolium chloride (C_4mimCl) molecules in hydrophobic benzyl alcohol is proposed. The templated TiO_2 powder, which incorporates phosphate species to enhance its structural stability, exhibits a small pore size of 4.2 nm and a high surface area of 164 $m^2\,g^{-1}$. Small amounts of the salts increase the ionic strength, slightly shrinking the template and the pore size, and pore expansion results when the salt/Ti ratio is above 0.2. The salts at a salt/Ti ratio of 1.0 remarkably extend the pore size to 8.7–16.8 nm in the order of NH_4NO_3 (16.8 nm) > NH_4Cl (13.7 nm) > $CaCl_2$ (12.4 nm) > NaCl (8.7 nm). Moreover, high surface areas of 154–199 $m^2\,g^{-1}$ are still achieved. The ions that have large radii and high valence numbers are more capable of expanding the pores because of strong volume exclusion and Coulomb repulsion. The critical pore size for the adsorption of hydrated bisphenol A molecules within the pores is ca. 4.2 nm. Pore expansion facilitates mass diffusion in the channels and turns internal surface areas available for reactions, thus greatly enhancing the activity of the mesoporous photocatalyst by 2.7–5.5 times.

1. Introduction

Titanium dioxide (TiO_2) is one of the most used photocatalysts for water and air purification because of its high photon-to-current conversion efficiency, high chemical stability and low toxicity [1,2]. A great deal of effort has been devoted to the construction of porous structures that increase the surface areas of photocatalysts for high activity. Surfactant-based templating method is commonly adopted to build up mesoporous structures [3,4]. By introducing amphiphilic substances into metal oxides and then removing them from the matrix, only voids with shapes similar to the templates remain.

Ionic liquids (ILs) are organic molten salts which are comprised of large organic cations and inorganic anions. Recently, ILs have been considered as a promising alternative to structural directing reagents in nanocasting [5,6]. Compared to traditional surfactants, their physicochemical features, including tunable solvent properties, adjustable polarities, and low vapor pressures, allow the salts more functionality in morphology control and more feasible for a variety of solvents and operating conditions. ILs, which serve as the templates for micro- and meso-open-framework materials, have been demonstrated. Cooper et al. [7] prepared zeolites in ILs and reported that the interaction of the negatively charged building blocks with the organic cations of the IL is the basis of the templating. Antonietti's group [8] used ILs consisting of 1-alkyl-3-methylimidazolium (abbreviated as $C_n$mim$^+$, where the n represents the number of carbon atoms in the alkyl chain) cations together with different anions to prepare highly ordered microporous or wormlike mesoporous silica. It is believed that the templating is a result of the self-assembly of the ILs through the π–π stacking interactions between the imidazolium rings and the hydrogen bonding between the inorganic anions and the metal oxides. The size of the anion determines the quality of the self-assembly of the ILs [9]. Large anions sterically hinder the organization of the imidazolium cation, and consequently resulting in wide pore-size distribution.

Zhou and Antonietti [10] prepared TiO_2 nanocrystals through hydrolysis of $TiCl_4$ in [C_4mim][BF_4]. Aggregation of the nanocrystals resulted in a mesoporous structure with an average pore size of 6.3 nm and a high surface area of 554 $m^2\,g^{-1}$. Yoo et al. [11] used four types of water immiscible ILs, including [C_4mim][PF_6],

* Corresponding author. Tel.: +886 3 5712121x55506; fax: +886 3 5725958.
E-mail address: chang@mail.nctu.edu.tw (S.-m. Chang).

0926-3373/$ – see front matter © 2012 Elsevier B.V. All rights reserved.
http://dx.doi.org/10.1016/j.apcatb.2012.11.026

[C_4mim][BF_4], [C_4mim][CF_3SO_3], and [C_6mim][PF_6] as the templates, to prepare mesoporous TiO_2 powders in a sol–gel process, and removed the templates using solvent extraction. They found that the [C_4mim][PF_6] exhibited the highest quality of templating behavior among these ILs, and resulted in a porous structure with a high surface area of 273 $m^2 g^{-1}$ and an average pore size of 4.5 nm. The CF_3SO_3 anion had the least capability for directing the mesoporous structures because its strong hydrogen bonding with hydrated metal oxides prevented the aggregation of the ILs from blocking the π–π stacking of the imidazolium rings. On the other hand, the C_6mim cation, which contains the longest alkyl chain, contributed to the largest pore size (ca. 8.0 nm) and pore volume (0.9 $cm^3 g^{-1}$). Thermal treatment is efficient for removing organic templates and crystallizing photocatalysts in order to promote high activity. However, porous materials are highly challenged by thermally induced pore collapse, which remarkably reduces their surface areas at elevated temperatures. The surface areas of IL-templated TiO_2 powders are generally smaller than 100 $m^2 g^{-1}$ after calcination at 500 °C, even though they are 253–478 $m^2 g^{-1}$ at 100 °C. By comparing the thermal stability of the porous TiO_2 powders prepared using [C_4mim][PF_6] and [C_4mim][BF_4], Choi et al. [12] found that the PF_6 anions were more capable of suppressing the solid-state aggregation of crystals and preserving the porous structures during the calcination than the BF_4 anions. In addition, they further used a non-ionic surfactant, Tween 80, as the co-template, and successfully increased the surface area of the [C_4mim][PF_6]-assisted sample from 96 to 215 $m^2 g^{-1}$ at 500 °C.

Mesoporous photocatalysts are basically fabricated to provide a large quantity of active sites for high reactivity. However, the contribution of surface area to reactivity is over-expected in some cases [12,13]. The [C_4mim][PF_6]-modified TiO_2 powder prepared by Choi et al. [12] showed a higher surface area (96 $m^2 g^{-1}$), but a lower photocatalytic activity than the unmodified sample (surface area: 71 $m^2 g^{-1}$). Han et al. [13] loaded dye molecules onto [C_4mim][BF_4]-templated TiO_2 electrodes and also found lower photo-to-current conversion efficiency on the electrodes with higher surface areas. They attributed the unexpected low performance to the small pore sizes which avoid the reactants entering the pore channels. Pore sizes, in fact, determine the mass diffusion within the pore channels and the effective surface areas for reactions [14,15]. The enhanced photocatalytic activities of TiO_2 photocatalysts that have large pore sizes or are loaded on the large-pored substrates have been demonstrated [16–18]. Pore-size-tailoring is of importance for the design of advanced catalysts. However, related approaches for IL-templated oxides have not been extensively developed.

For the first time, in this study, inorganic salts are used as the auxiliary agent to easily adjust the pore size of IL-templated TiO_2 photocatalysts. The presence of the salts in the hydrophobic benzyl alcohol (BA) medium assists the self-assembly of water-miscible C_4mimCl molecules into micelle-like aggregates, and controls the size of the IL-aggregates based upon their concentrations and the radii and charges of the constituent ions. To enhance the stability of the porous structures during thermal treatment, phosphate species is incorporated into the TiO_2 surface lattice. We have successfully enlarged the pore size of the templated TiO_2 photocatalysts from 4.2 to 8.7–16.8 nm through the addition of four types of salts, including NH_4NO_3, NH_4Cl, $CaCl_2$ and NaCl. Moreover, large surface areas of 154–199 $m^2 g^{-1}$ are maintained. We clearly demonstrate that the pore expansion effectively improves the photocatalytic activities of the mesoporous TiO_2 samples for the degradation of bisphenol A (BPA). The pore-size-dependent activities are understood in terms of their adsorption behavior.

2. Experimental

2.1. The IL-templated sol–gel process

Porous TiO_2 powders were prepared using a sol–gel process in the presence of IL molecules in a benzyl alcohol (BA, Sigma–Aldrich, 99.0%) medium. Titanium tetra-isopropoxide (TTIP, Acros, 98.0%) and 1-butyl-3-methylimidazolium chloride (C_4mimCl, Sigma–Aldrich, >95.0%) were dissolved into the BA solvent with vigorous stirring, followed by addition of HCl (JT Baker, 36.5%) and H_3PO_4 (Sigma–Aldrich, 85.0%) to initiate the sol–gel reaction. The molar ratio of these reagents was fixed as TTIP:C_4mimCl:BA:HCl:H_3PO_4 = 1.0:1.0:30:25:1.0. The sol solution was heated at 70 °C under constant stirring for 24 h to evaporate the solvent and induce the self-assembly of the TiO_2 colloids and the IL molecules. The resulting powders were dried at 150 °C to increase their condensation level. Prior to the calcination for the template removal, the powders were washed three times with methanol. The IL-templates were burned out in air using a heating program: the temperature was increased from room temperature to 550 °C at a rate of 10 °C min^{-1} and kept at 550 °C for 5 h. To adjust the textures of the porous TiO_2 sample, NaCl, $CaCl_2$, NH_4Cl, and NH_4NO_3 salts were added to the sol solution, with a salt/Ti ratio of 0.1–1.0.

2.2. Characterization

Nitrogen adsorption/desorption isotherms were measured using a gas sorption analyzer (Micromeritics, Tristar 3000) at 77 K. The Brunauer–Emmett–Teller (BET) model was used to estimate the surface areas of the samples based on the adsorption data. Pore-size distribution and pore volume were derived from the desorption branch and calculated by using the Barrett–Joyner–Halenda (BJH) model. Before the measurement, the samples were heated at 130 °C under vacuum for 12 h to remove adsorbed water and volatile contaminants. The morphology of the porous powders was examined by using a high-resolution transmission electron microscope (HR-TEM, Phillip TECNAI 20) operated at an accelerating voltage of 200 kV. The elemental compositions and states at the surface were determined using an X-ray photoelectron spectrometer (XPS, Physical Electronics, ESCA PHI 1600) with Al Kα radiation (1486.6 eV). The photoelectrons were collected into the analyzer with a pass energy of 23.5 eV and at a collection step of 1.0 and 0.1 eV, respectively, for wide and high-resolution scans. Chemical shifts resulting from charging effects were calibrated by fixing the C 1s peak of the surface carbonaceous contaminants at 284.8 eV. The crystalline structures of the TiO_2 powders were examined using an X-ray powder diffractometer (XRPD, Brucker D2 phaser) with Cu Kα radiation (λ = 1.5406 Å), an accelerating voltage of 30 kV, and an emission current of 10 mA. Diffraction patterns were recorded at the 20–80° 2θ positions with a sampling width of 0.03° and a scanning speed of 11° min^{-1}. The band gaps of the samples were analyzed using UV–Vis spectrometry (HITACHI 3010) in a diffused reflectance mode with a scanning range from 700 to 200 nm. Aluminum oxide (Al_2O_3), which is considered to exhibit total reflection, was used as the reference for all measurements. The diffused reflectance was then converted into absorptions using the Kubelka–Munk formula [19].

2.3. Photocatalytic activity

The photocatalytic activities of the porous TiO_2 photocatalysts were examined in terms of degradation of 20 mg l^{-1} BPA aqueous solution under illumination of UV light at 305 nm. Prior to the illumination, the TiO_2 suspension (1.0 g l^{-1}) was purged with O_2 for 60 min to reach a saturated state. Meanwhile, the adsorption/desorption of BPA and O_2 molecules on the TiO_2

surface achieved an equilibrium in the darkness. The photocatalytic degradation of BPA molecules was examined by analyzing their remaining concentration in the TiO_2 suspension sampled at different time intervals after illumination. To remove the TiO_2 photocatalyst, the suspension was centrifuged at 10,000 rpm for 5 min. The BPA concentrations were analyzed using a high performance liquid chromatograph (HPLC, Waters Alliance 2695) equipped with a C18 column (5 μm, 4.6 mm × 250 mm) and a photodiode array detector (PDA, Waters 2996). The mobile phase was a methanol–water mixture (80/20, V/V) at a flow rate of 1.0 ml min^{-1}. The photocatalytic activities of the TiO_2 photocatalysts were represented by the rate constants derived from the degradation curves using the Langmuir–Hinshelwood model.

2.4. Adsorptions

Adsorption tests were carried out in a series of vials in the darkness. The dosage of the TiO_2 powders and the initial concentration of BPA were fixed at 1.0 g l^{-1} and 20 mg l^{-1}, respectively, in all the vials. The TiO_2 suspensions were sampled from the vials sequentially after different time intervals and centrifuged to remove the powders. The BPA concentrations in the supernatants were measured using the LC to calculate the adsorbed amounts.

3. Results and discussion

3.1. IL-templated TiO_2 photocatalysts

Fig. 1 shows the N_2 adsorption/desorption isotherms and the corresponding pore-size distributions of the non-templated and IL-templated TiO_2 samples. Type IV adsorption curves with hybrid H2–H3 hysteresis loops were observed in these two samples, indicating their mesoporous structures. The non-templated TiO_2 powders had a mean pore size (D_m) of 6.6 nm, and the pore size was extended to 8.7 nm in the presence of the C_4mimCl molecules. Both the non-templated and IL-templated TiO_2 samples exhibited wide pore-size distributions, small pore volumes (V_p: 0.11–0.26 cm^3 g^{-1}) and low specific surface areas (SA: 45–56 m^2 g^{-1}). These were the consequence of sintering and crystallization, which rearrange the elements and collapse the pores. Phosphation of TiO_2 powders has been demonstrated to inhibit the elemental rearrangement in the oxide [1,2]. To enhance the thermal stability of the porous structure, phosphate species was incorporated into the TiO_2 lattice via the addition of phosphoric acid into the sol–gel reaction. This doped TiO_2 sample is called P-TiO_2. The templated P-TiO_2 powder ended its hysteresis loop at a lower P/P_0 value (0.4) compared to the pure TiO_2 samples (P/P_0 = 0.6–0.7), indicating smaller pore sizes (see Fig. 1). A narrow pore-size distribution with a D_m of 4.2 nm and a high SA of 164 m^2 g^{-1} were obtained after the phosphation.

In addition to the structural stabilization, the phosphoric acid helps the aggregation of the IL molecules in the BA medium. At 350 °C, which was still a low enough temperature to induce significant structural transformation, the P-TiO_2 sample also showed a smaller pore size (3.4 nm) and a larger specific surface area (341 m^2 g^{-1}) than the templated TiO_2 powders (D_m: 9.0 nm, SA: 155 m^2 g^{-1}). This phenomenon reveals that a higher templating level resulted in the phosphated system. Fig. 2 displays the proposed mechanism of the self-assembled C_4mimCl molecules in the BA medium and the salt-assisting processes. The π–π stacking and non-covalent interactions between the imidazolium rings and butyl chains are believed to drive the self-assembly of the C_4mimCl molecules into micelle-like aggregates. The aggregates template the porous structures of the TiO_2 samples through the electrostatic attraction with the hydrated colloids. The phosphoric acid increases the ionic strength of the solution, thus triggering

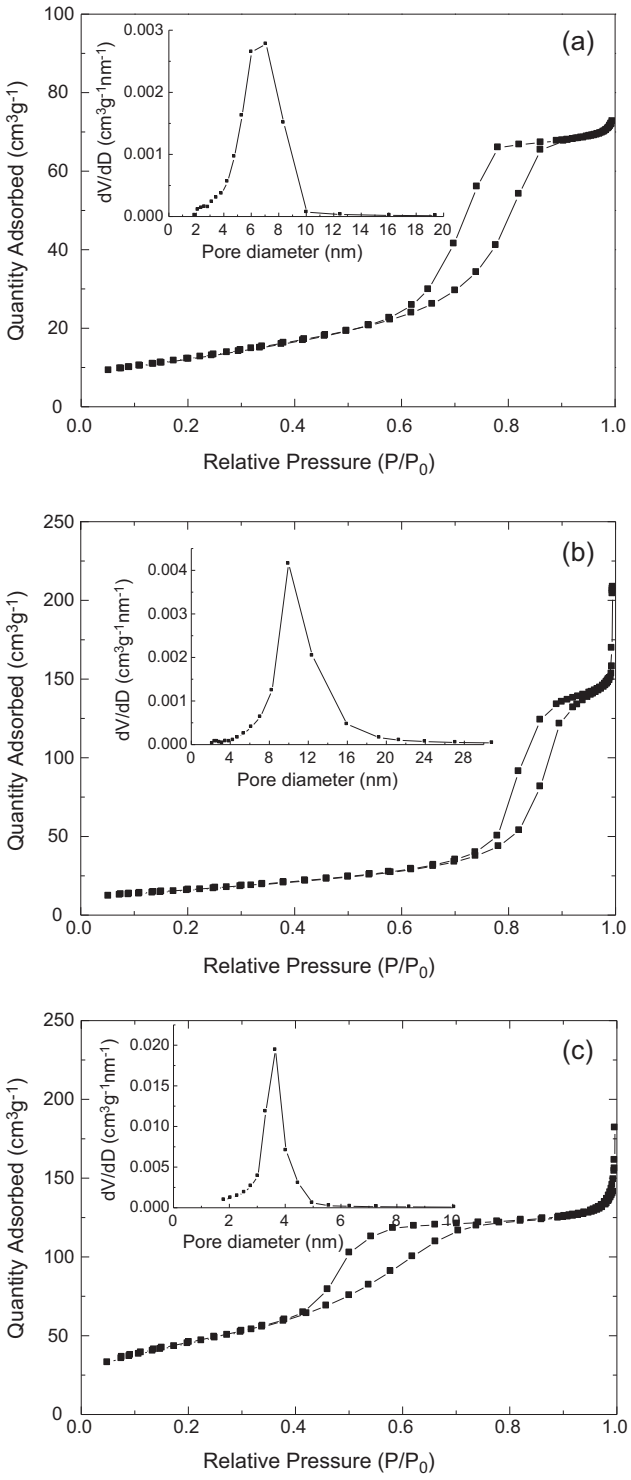

Fig. 1. The N_2 adsorption/desorption isotherms and the corresponding pore-size distributions of the (a) non-templated, (b) IL-templated TiO_2 and (c) IL-templated P-TiO_2 samples.

the separation of the water-miscible IL from the hydrophobic BA medium to form denser and more well-defined aggregates. Moreover, chelation of the phosphate ions to the Ti^{4+} centers inhibits the growth of the colloids. It is easier to orient the small colloids along with the templates and achieve high templating quality. Hereafter, the phosphated sol–gel system is exploited to study the effects of inorganic salts on pore-size tailoring.

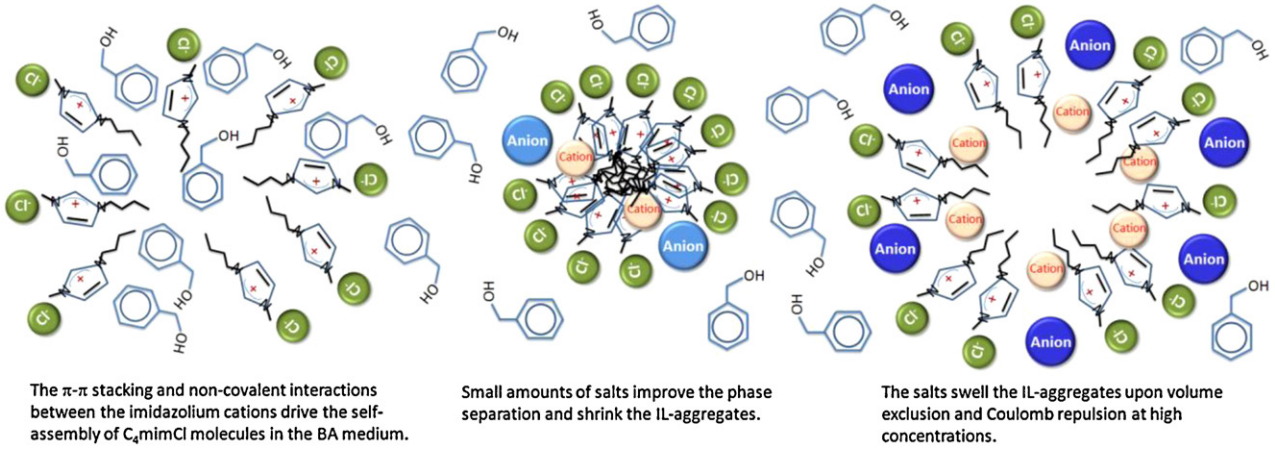

Fig. 2. The self-assembly of the C_4mimCl molecules in the BA medium and the salt-induced shrinkage and expansion of the IL-aggregates.

3.2. Salt-assisted pore-size expansion

Inorganic salts, which are less soluble in the BA medium, were used as the auxiliary reagents to enlarge both the IL-aggregates as well as the pore sizes of the templated TiO_2 samples. Fig. 3 shows the pore-size distributions of the templated P-TiO_2 samples prepared in the presence of NH_4Cl, NH_4NO_3, $CaCl_2$, and NaCl salts at a salt/Ti ratio of 1.0. The salts obviously shifted the major pore size of the templated P-TiO_2 sample from 3.6 to 8.6–10.1 nm and broadened the size distributions. Table 1 summarizes the textural data of the P-TiO_2 powders prepared with and without the salts. The salts significantly extended the D_m of the P-TiO_2 sample from 4.2 to 8.7–16.8 nm in the order of NH_4NO_3 (16.8 nm) > NH_4Cl (13.7 nm) > $CaCl_2$ (12.4 nm) > NaCl (8.7 nm). Correspondingly, the V_p was increased from 0.23 to 0.37–0.82 $cm^3\ g^{-1}$. High surface areas in the range of 154–199 $m^2\ g^{-1}$ were maintained in the salt-assisted templating system, indicating that the expanded pore sizes mainly resulted from the enlarged templates.

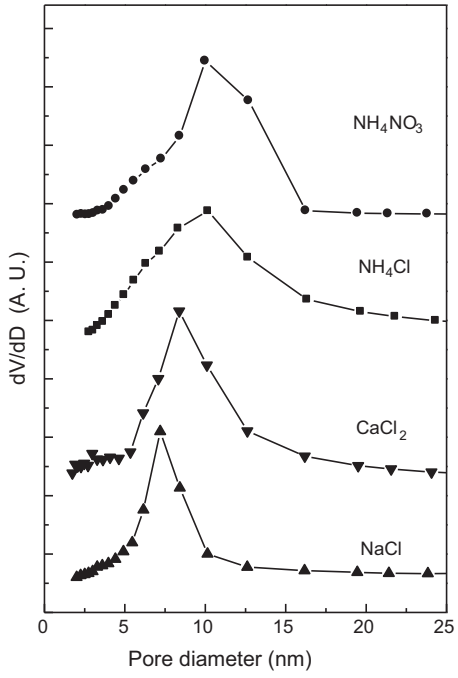

Fig. 3. The pore-size distributions of the templated P-TiO_2 samples prepared in the presence of NH_4Cl, NH_4NO_3, $CaCl_2$, and NaCl salts.

Pore expansion in the surfactant-directed templating system is usually conducted based on oil-in-water emulsions. Encapsulation of hydrophobic additives, including trialkylbenzenes, alkanes, and alkyl alcohols, into the micelles swells the micelle size, leading to large pores in the templated materials [20]. The size and solubility of the organic expanders in the oil-like cores of micelles determine the expansion capability [21]. Pore-size tailoring is little addressed in IL-templated systems. Yoo et al. [11] used water-immiscible ILs as templates for mesoporous TiO_2 powders and found that the pore size increased from 4.5 to 8.0 nm when the carbon number of the alkyl chain in the cationic part increased from 4 to 6. Hu et al. [22] used C_4mimBr together with equal amounts of CTAB as the co-template to prepare porous silica. Via increasing preparation temperature from 303 to 373 K, they slightly increased the pore size from 2.0 to 2.7 nm. In this study, for the first time, inorganic salts are used as the expanders for pore-size tailoring in IL-templated systems. Moreover, we have demonstrated that the salt-assisted approach is effective for pore expansion, and even more facile and economical than the conventional strategies. The interactions of the salts with the IL-aggregates for expanding the template is shown in Fig. 2. Ionic features allow the salts to better dissolve in the IL-aggregates rather than be mixed with the BA solvent. The additional anions and cations from the salts are inserted interstitially in the ionic layers of the IL-aggregates to increase their size. According to Pauling's rule, the ionic radii of Na^+, Ca^{2+}, NH_4^+, Cl^-, and NO_3^- ions are 95, 99, 148, 181, and 264 pm, respectively [23]. The NH_4Cl salt resulted in a larger pore size (13.7 nm) than the NaCl (8.7 nm) because the NH_4^+ ion has a larger radius than the Na^+ ion. The NH_4NO_3 salt, which combines both the largest cation and the largest anion, extended the pore size the most (16.8 nm). Hydrated ionic radii are not considered for the pore-size control since all the as-prepared powders have been dried at 150 °C prior to calcination. The cations and anions have different capabilities for pore expansion. Compared the pore size resulting from the NaCl salt with that

Table 1
The textural data of the templated P-TiO_2 samples prepared in the absence of and in the presence of different inorganic salts.

Inorganic salt	D_m [nm][a]	V_p [$cm^3\ g^{-1}$][b]	SA [$m^2\ g^{-1}$][c]
NH_4NO_3	16.8	0.82	170
NH_4Cl	13.7	0.79	183
$CaCl_2$	12.4	0.60	199
NaCl	8.7	0.37	154
None	4.2	0.23	164

[a] Mean diameter.
[b] Pore volume.
[c] Specific surface area.

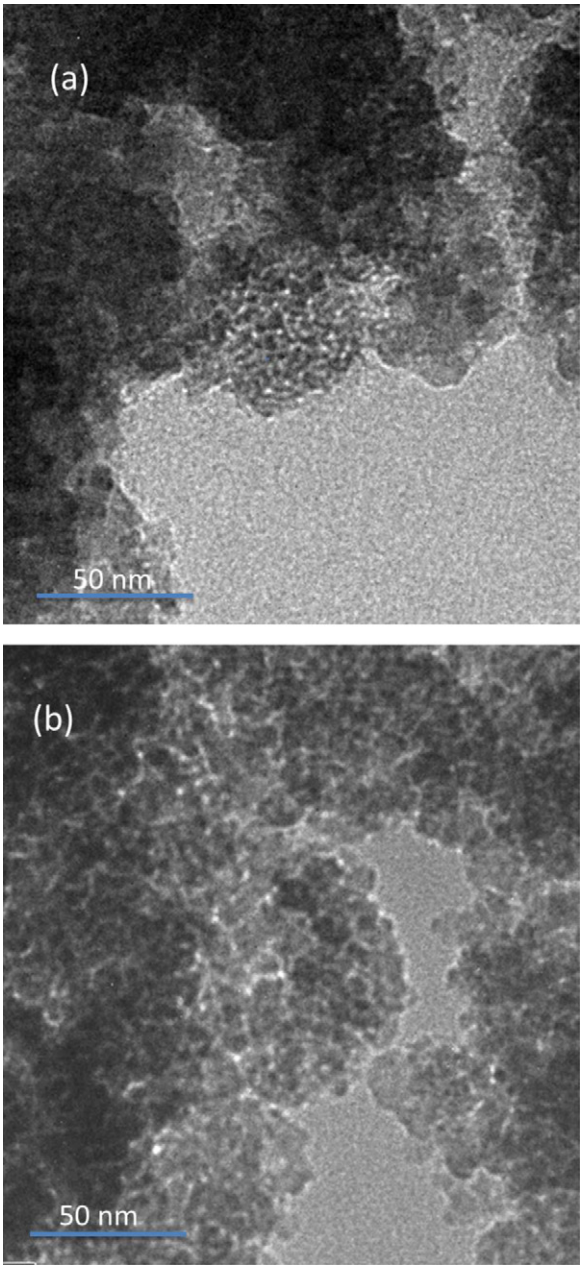

Fig. 4. TEM images of (a) P-TiO_2 and (b) P-TiO_2-NH_4NO_3 powders.

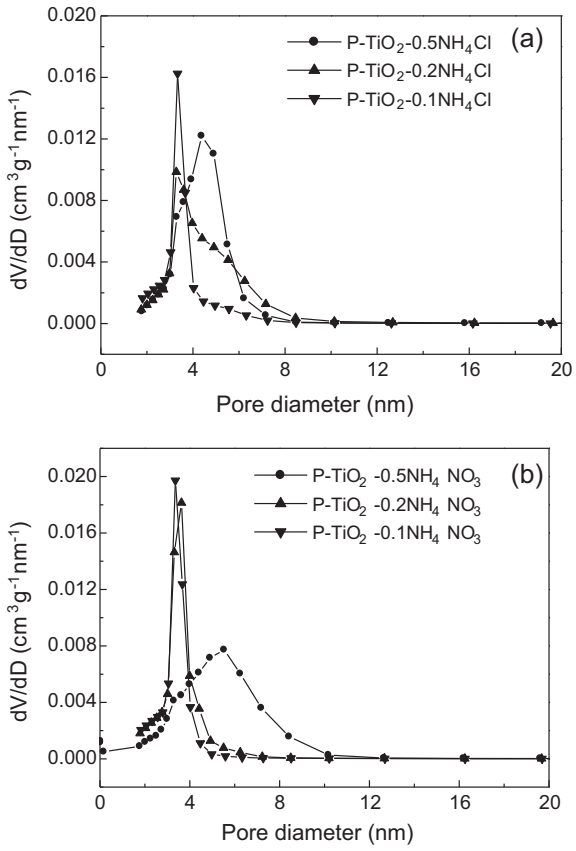

Fig. 5. The pore-size distributions of the P-TiO_2 samples prepared with different concentrations of NH_4Cl and NH_4NO_3 salts.

from the NH_4Cl salt, the pore size increased by 5.0 nm when the cationic radii increased by 53 nm. On the other hand, only 3.1 nm of increment in the pore size was obtained when the NH_4Cl was replaced by the NH_4NO_3, where the NO_3^- anion is 83 nm larger than the Cl^- anion. This finding indicates that incorporation of the cations into the imidazolium core is more effective than inserting the anions into the outer shell for expanding the IL-aggregates. The Ca^{2+} (99 pm) and the Na^+ (95 pm) ions have similar ionic radii. However, the resulting pore size (12.4 nm) from the $CaC1_2$ salt was distinctly larger than the size resulting from the NaCl salt. The higher valent number of the Ca^{2+} ions, which are able to induce stronger Coulomb repulsion to significantly swell the core of the template, is mainly responsible for the high extent of the pore expansion, even though the higher numbers of Cl^- anions from the $CaCl_2$ also expand the outer shell of the aggregates. Fig. 4 shows the TEM images of the P-TiO_2 and the P-TiO_2-NH_4NO_3 powders. It can be seen that continuous connection of the TiO_2 particles forms the interstitial pores. The NH_4NO_3 salt enlarges the pore size, but causes irregular pore shape in the meantime. Incorporation of the salt into the IL-aggregates separates the IL molecules from each other. The reduced interactions between the imidazolium cations cause the aggregates to no longer be confined to their shapes. This is also the reason for the broadening of the pore-size distributions in the salt-assisted samples.

Fig. 5 shows the pore-size distributions of the P-TiO_2 samples prepared using different concentrations of NH_4Cl and NH_4NO_3 salts. The corresponding textural results are listed in Table 2. The NH_4Cl and NH_4NO_3 salts increased the mean pore sizes from 3.6 to 5.8 nm and from 3.6 to 5.1 nm, respectively, when the salt/Ti ratios increased from 0.1 to 0.5. Compared to the textural results in the absence of the salts (D_m = 4.2 nm, FWHM of the pore-size distribution = 0.7 nm), narrower pore-size distributions (FWHM = 0.4–0.5 nm) and smaller pore sizes (3.6 nm) were found when the salt/Ti = 0.1. A little amount of the salts increases the

Table 2
The textural data of the templated P-TiO_2 samples prepared with the NH_4Cl and NH_4NO_3 at different concentrations.

Salt	Salt/Ti	D_m [nm][a]	V_p [$cm^3\ g^{-1}$][b]	SA [$m^2\ g^{-1}$][c]
NH_4Cl	0.5	5.8	0.40	208
	0.2	4.4	0.26	177
	0.1	3.6	0.17	147
NH_4NO_3	0.5	5.1	0.32	194
	0.2	3.9	0.22	186
	0.1	3.6	0.21	170

[a] Mean diameter.
[b] Pore volume.
[c] Specific surface area.

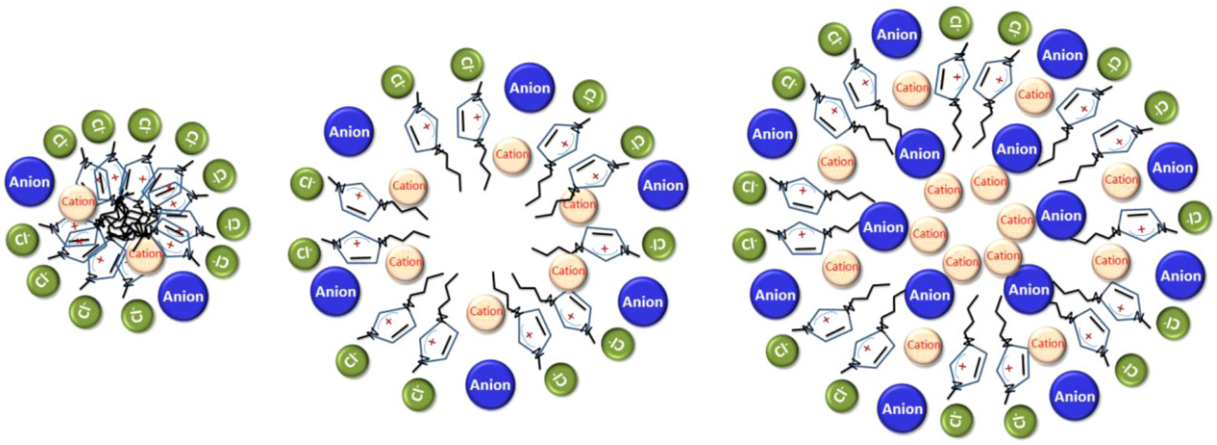

Fig. 6. The swollen IL-aggregates with increasing concentrations of the salts.

ionic strength in the IL-aggregates, thus repelling the BA solvent from the aggregates and shrinking them (see Fig. 2). Similar pore shrinkage was also found when phosphate ions were involved in the self-assembly. The salts started to effectively expand the pore sizes when the salt/Ti ratio was larger than 0.2. The pore volumes increased from 0.17–0.21 to 0.79–0.82 $cm^3\ g^{-1}$ when the salt/Ti ratio increased from 0.1 to 1.0 as a result of the pore expansion. The specific surface areas (147–208 $m^2\ g^{-1}$) positively correlated to the salt concentrations when the salt/Ti = 0.1–0.5. In turn, they declined from 194–208 to 170–183 $m^2\ g^{-1}$ when the salt/Ti ratio was further increased to 1.0. To understand the effect of the salt concentrations on the textures, we calculated the numbers of templated pores from the pore volumes (V_p, $cm^3\ g^{-1}$) and the pore sizes (D_m, nm). Assuming each pore has perfectly cylindrical shapes and the same length (L, nm), the numbers of pores (N) can be calculated from the following equation:

$$N = \frac{V_p \times 10^{21}}{(D_m/2)^2 \pi \times L} \quad (1)$$

Because the length is unknown, we take the numbers at the salt/Ti = 0.1 as the base value to estimate the relative values. The relative numbers of pores are 1.05, 0.93, and 0.33 for the salt/Ti = 0.2, 0.5, and 1.0, respectively, in the NH_4Cl-assisted system, and are 0.91, 0.77, and 0.18, respectively, in the presence of the NH_4NO_3 salt. The numbers drop significantly at the salt/Ti = 1.0, explaining the reduced surface areas at high concentrations of the salts. Moreover, it implies the existence of a maximum salt/IL ratio for stabilizing the IL-aggregates. Over the ratios, the amounts of the IL molecules are too low to generate sufficient attraction for gathering. The IL molecules tend to rearrange themselves into a large aggregate and segregate the inorganic ions to the core, so that the density of the IL molecules in the shell can be maintained at a sufficient level to confine them. The influence of salt concentrations on the self-assembly of IL molecules is illustrated in Fig. 6.

3.3. Surface and crystalline characterizations

Fig. 7 shows the XP spectra of the P-TiO_2 samples prepared both in the absence of and in the presence of the salts where the salt/Ti = 1.0. All P-TiO_2 samples contained Ti, O, and P photoelectron lines in their spectra. The P/Ti atomic ratios, which were in the range of 0.76–1.25, were higher than the added ratio (P/Ti = 0.3), indicating that the phosphate species is mainly doped within the surface lattice. The Ca and Na species with Ca/Ti and Na/Ti ratios of 1.85 and 1.71, respectively, were additionally detected in the P-TiO_2-$CaCl_2$ and P-TiO_2-NaCl samples. A similar manner to the phosphate species, the Ca/Ti and Na/Ti ratios that are higher than the added values (salt/Ti = 1.0) reveal the accumulation of these two ions on the surface. The Ca $2p_{2/3}$ and Ca $2p_{1/2}$ lines centered at 347.6 and 351.2 eV, respectively, indicating a $Ca_3(PO_4)_2$ species [24] (see the Supplementary Material, Figure S1). On the other hand, the Na 1s peak at 1071.9 eV denotes a $NaPO_3$ species in the TiO_2 matrix [25,26] (see the Supplementary Material, Figure S1). These results reveal that both the Ca^{2+} and Na^+ ions preferentially bond to the phosphate species rather than to the $Ti(OH)_4$ colloids during the sol–gel process. In contrast to the deposition of the Ca^{2+} and Na^+ ions, N elements were not detected in the P-TiO_2-NH_4NO_3 and P-TiO_2-NH_4Cl samples. By using NH_4Cl as the N source, Reyes-Gil et al. [27] incorporated NH_x and NO_3^- into the interstitial sites of TiO_2 and In_2O_3 crystals. Sun et al. [28] used NH_4Cl salt to prepare N-doped TiO_2 samples under different pH values and found that the concentration of the doped N species decreased with decreasing

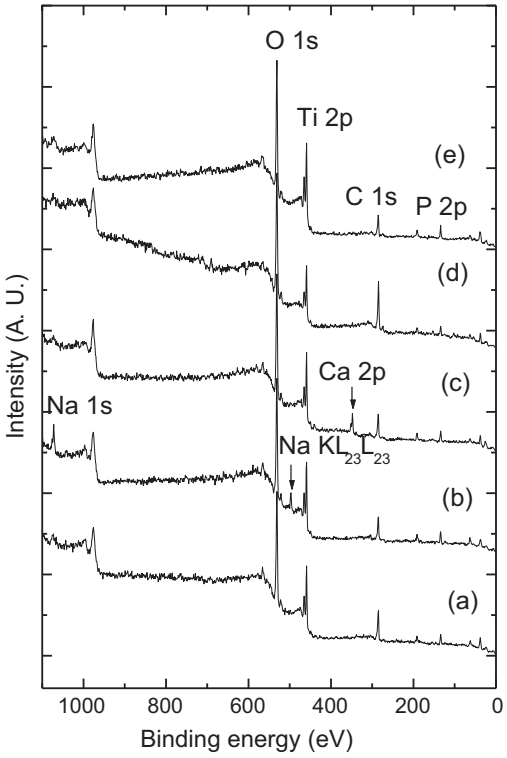

Fig. 7. The XP spectra of the (a) P-TiO_2, (b) P-TiO_2-NaCl, (c) P-TiO_2-$CaCl_2$, (d) P-TiO_2-NH_4Cl, and (e) P-TiO_2-NH_4NO_3 samples.

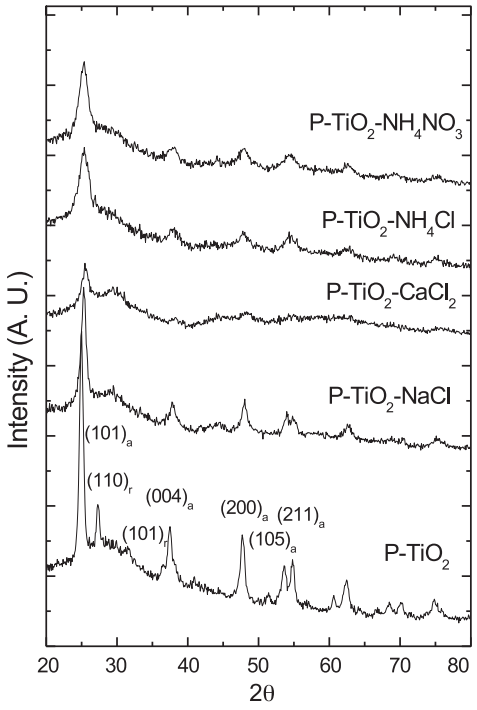

Fig. 8. The XRD patterns of the P-TiO_2, P-TiO_2-NaCl, P-TiO_2-$CaCl_2$, P-TiO_2-NH_4Cl, and P-TiO_2-NH_4NO_3 samples.

pH values. The doping mechanism is based on formation of $Ti(H_2O)_5NH_3$ complex. In this study, N-doped TiO_2 samples were unavailable even though the C_4mim, NH_4^+, and NO_3^- ions contain N elements. The protonation under acidic conditions and the intrinsic cationic properties make it difficult for the ions to chelate to the Ti^{4+} centers and inhibit the doping process. These N-contained species are burned out from the samples during the calcination in terms of the formation of NO_x gases.

Supplementary data associated with this article can be found, in the online version, at http://dx.doi.org/10.1016/j.apcatb.2012.11.026.

The XRD patterns of these porous TiO_2 samples are shown in Fig. 8. The original P-TiO_2 powders were crystallized into anatase and rutile forms with the mass ratio of 82/18. Addition of the inorganic salts suppressed the crystallization and the formation of the rutile phase. The average size of the anatase crystals was 12 nm in the P-TiO_2 powder, which decreased to 5–10 nm in the salt-assisted samples. It is noted that the salt-assisted powders showed lower surface P/Ti ratios (0.76–0.89) than the original sample (P/Ti = 1.25), thus the suppressed crystallization was attributed to the high concentration of impurities in the bulk. The band gaps of these P-TiO_2 powders were in the range of 3.12–3.30 eV (see the Supplementary Material, Figure S2). The presence of the impurities in the TiO_2 lattice did not significantly reduce the band gap, implying that the energy levels of the impurities located within the bands.

Supplementary data associated with this article can be found, in the online version, at http://dx.doi.org/10.1016/j.apcatb.2012.11.026.

3.4. Photocatalytic activity

The photocatalytic activities of the P-TiO_2 samples were examined in terms of the degradation of 20 mg l^{-1} BPA under illumination of UV light at 305 nm. Fig. 9 shows the degradation curves of BPA in the presence of the original and pore-expanded P-TiO_2 samples. The degradation follows pseudo-first

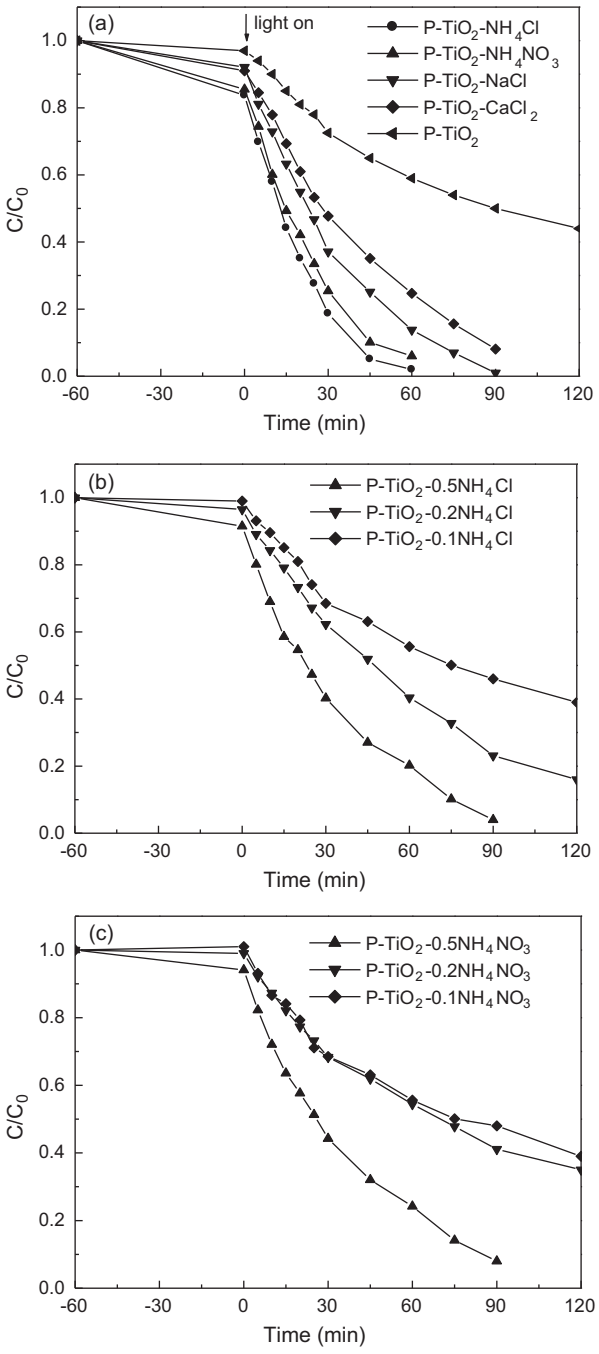

Fig. 9. The degradation curves of BPA in the presence of (a) the P-TiO_2 photocatalysts prepared both without and with various salts at salt/Ti = 1.0. (b) and (c) are the degradation induced by the NH_4Cl- and NH_4NO_3-assisted samples with different salt/Ti ratios, respectively.

order kinetics. The photocatalysts with the salt/Ti = 1.0 showed that the rate constant (k) was in the order of the P-TiO_2-NH_4Cl ($k = 4.58 \times 10^{-2}$ min^{-1}) > the P-TiO_2-NH_4NO_3 ($k = 3.80 \times 10^{-2}$ min^{-1}) > P-TiO_2-NaCl ($k = 2.98 \times 10^{-2}$ min^{-1}) > P-TiO_2-$CaCl_2$ ($k = 2.21 \times 10^{-2}$ min^{-1}) > P-TiO_2 ($k = 8.30 \times 10^{-3}$ min^{-1}). Although the salt-assisted samples had poorer crystallinity, and some of them contained substantial amounts of additional deposits ($Ca_3(PO_4)_2$ and $NaPO_3$) from the salts, they all exhibited higher activities than the original sample. From the results, it is obvious that pore expansion contributes to the enhanced activities. On the other hand, significant adsorptions were also found in the pore-expanded TiO_2 suspensions after 60 min of equilibrium in

the darkness. The P-TiO_2-NH_4Cl and P-TiO_2-NH_4NO_3 photocatalysts reduced the concentration of the BPA by 14–16% through adsorption, followed by the P-TiO_2-$CaCl_2$ and P-TiO_2-NaCl photocatalysts which decreased the initial concentration by 8.0–9.0%. The adsorption of BPA was negligible in the original P-TiO_2 suspension. The samples prepared with different concentrations of NH_4NO_3 and NH_4Cl salts showed increased photoactivities (from 9.55×10^{-3} to 2.62×10^{-2} min^{-1}) and adsorption amounts (from 0.40 to 1.60 $mg\,g^{-1}$) with their increasing salt/Ti ratios (from 0.1 to 0.5), and, correspondingly, with their increased pore sizes (from 3.6 to 5.8 nm). These results imply that there is correlation among the photocatalytic activities, the adsorption capability and the pore sizes. Photocatalysis is considered to follow the Langmuir–Hinshwood mechanism, which claims that reactions only take place on the surface after adsorptions. We have demonstrated the adsorption-improved photocatalytic kinetics on the surface modified TiO_2 photocatalysts in our earlier work [1]. To insightfully understand the pore-size-dependent activity in this study, we further examine the adsorption behavior of the porous TiO_2 samples in the darkness.

The adsorption curves show that the equilibrium was reached within 30 min in all sets (see Supplementary Material, Figure S3). The tangent values of the adsorption curves within the first 10 min are determined as the adsorption rates. Fig. 10 shows the photocatalytic activities, adsorption capability, and adsorption rates of the porous P-TiO_2 powders against their pore sizes. In spite of having large surface areas, the samples that had pore sizes smaller than 4.2 nm exhibited poor photocatalytic performance and little adsorption (0.4–0.5 $mg\,g^{-1}$). Such low photocatalytic activities are mainly restricted by the limited adsorptions on the external surface of the porous powders. Surface tension and size exclusion limit the diffusion of BPA molecules into the small pore channels [29,30]. Although the BPA molecule is only 1.1 nm in length [31], the coagulation from the π–π stacking between the phenyl groups, together

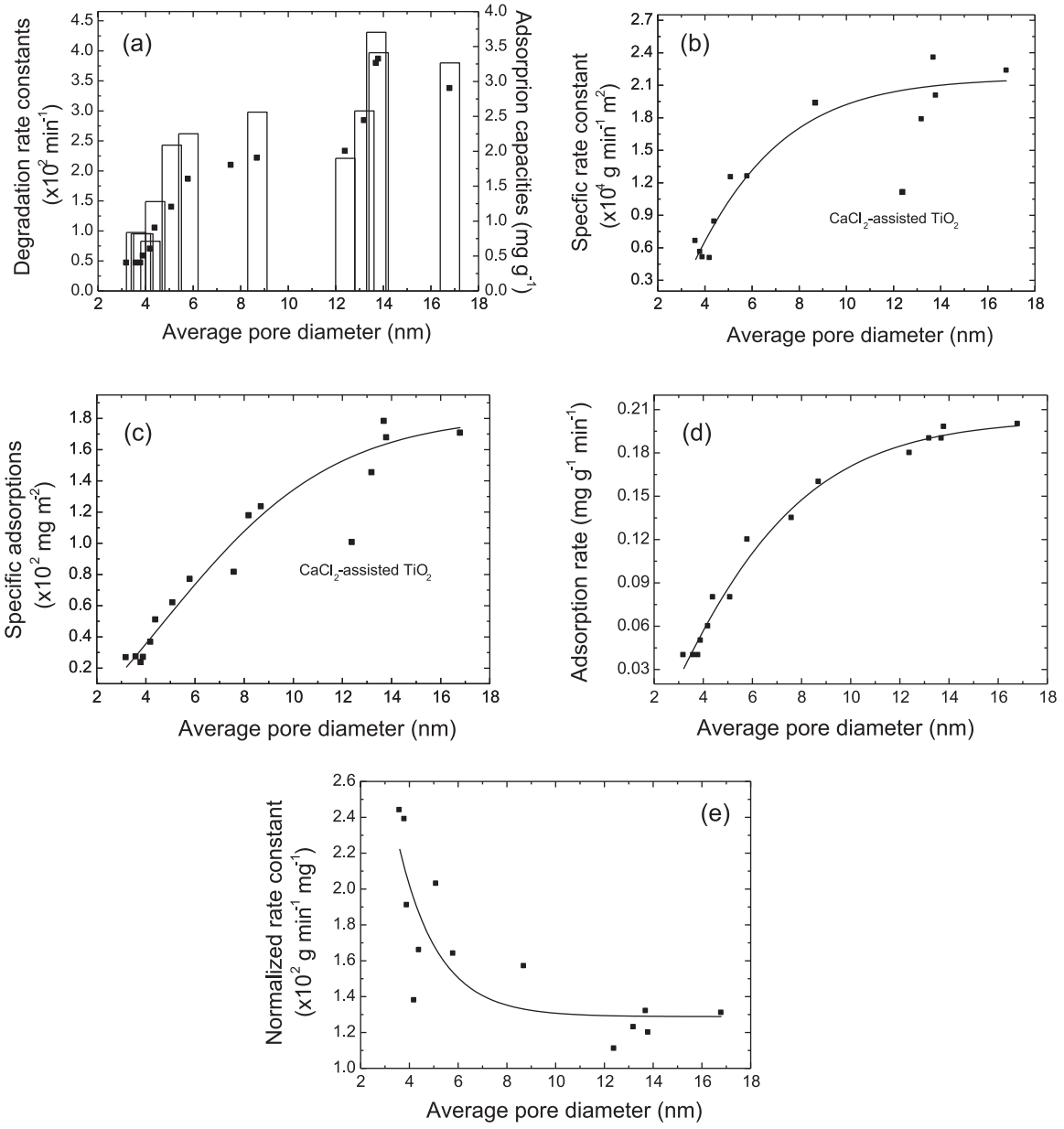

Fig. 10. (a) The degradation rate constants (bars) and adsorption capacities (■), (b) the specific rate constants, (c) specific adsorption capacities, (d) adsorption rates, and (e) the normalized rate constants of the porous P-TiO_2 samples against their average pore sizes.

with hydration significantly increases the size of the hydrated clusters. In this study, the critical pore size that is able to accommodate the hydrated BPA clusters is about 4.2 nm. Remarkably, the degradation rate constants as well as the adsorption capacities increased with increasing pore sizes when the pore sizes were larger than the critical pore size (4.2 nm). To eliminate the contribution of surface areas to the apparent reactivity and adsorptions, we further normalized the rate constants and the adsorption capacities with their specific surface areas. The specific rate constants increased steeply with the pore sizes until 8.7 nm and almost reached a plateau in the range of 13.0–16.8 nm (Fig. 10b). Similar trends were found in the pore-size-dependent specific adsorption capacities and adsorption rates (Fig. 10c and d). These findings clearly indicate that expanded pores open the internal surface areas of the porous catalysts to the BPA molecules and facilitate their diffusion within the pore channels, thereby improving the photocatalytic activities. When the specific adsorption capacity reaches saturation and the adsorption rate achieve the highest value, the effects of pore sizes on the reactivity diminish gradually. In turn, surface areas of catalysts dominate the activities. This situation takes place when the pore sizes are larger than 13.0 nm. The P-TiO_2-$CaCl_2$ powder exhibited a relatively lower specific activity compared to the samples having smaller pore sizes. Its lower adsorption capacity reveals that the $Ca_3(PO_4)_2$ species decreases the reactivity as a consequence of suppressing the BPA adsorptions. Regarding the influence of mass transfer on the photocatalytic efficiency, we normalized the rate constants with the adsorption capacities (Fig. 10e). The normalized rate constants decrease dramatically when the pore size increases to 4.2 nm. The slope become gentle in the range of 4.2–8.7 nm, and is almost flat over 13.0 nm. This phenomenon again proves that the chemical reactions on the external surface of the porous catalysts dominate the photocatalytic kinetics when the pore size is smaller than the critical size. When the pore size is large enough to accommodate BPA molecules in the pore channels, pore expansion remarkably reduces steric hindrance and raises the importance of inside-pore reactions. Under this condition, frictional hindrance determines the mass transfer in the channels and in turn controls the photocatalytic kinetics [32]. Both the lowest normalized and the highest specific rate constants occur when the pore size is in the range of 13.0–16.8 nm. It is expected that the weight of frictional hindrance reduces when the pores size is larger than 16.8 nm, and photocatalytic activity of the porous TiO_2 catalysts can be further improved.

Supplementary data associated with this article can be found, in the online version, at http://dx.doi.org/10.1016/j.apcatb.2012.11.026.

Many studies have demonstrated the enhanced activity of porous materials and claimed the improvement as the result of high surface areas. However, the contribution of the measured surface areas to the activity may have been over-estimated if the availability of the internal surface for the reactants and the mass transfer in the pores were not considered. In this study, we use inorganic salts to effectively expand the pore size of the IL-templated mesoporous TiO_2 photocatalysts from 4.2 to 16.8 nm and demonstrate their improved photocatalytic activities with increasing pore sizes. Moreover, the critical pore size for BPA diffusion in the pores is determined. These results not only provide a novel approach for texture control of catalysts, but also extend the knowledge of the photocatalytic kinetics beyond textures.

4. Conclusions

We have successfully adjusted the pore sizes of the C_4mimCl-templated TiO_2 powders through the novel salt-assisted approach. The pore-size tailoring is controlled by the radii, the charges, and the concentrations of the constituent ions based on the volume exclusion, the Coulomb repulsion, and the ionic strength induced by the salts in the IL-aggregates. Small amounts of the salts increase the ionic strength to result in denser and smaller aggregates in the hydrophobic BA medium. Incorporation of the ions with high concentrations into the aggregates swells the templates and expands the templated pore size. The salts, which are comprised of ions with large ionic radii and high valence numbers, induce strong volume exclusion and Coulomb repulsion and are more capable of enlarging the pores. As the IL-aggregates swell, reduced interactions between the IL molecules also result in broad pore-size distributions and irregular pore shapes. A minimum IL-interaction is required for stabilization of the aggregates. Once the concentrations of the salts are too high, the ions tend to segregate into the core of the aggregate to maintain sufficient interactions in the shell. The photocatalytic reactivity of the porous TiO_2 sample is greatly promoted by 2.7–5.5 times when its pore size is expanded from 4.2 to 16.8 nm. Pore expansion reduces steric hindrance to facilitate the diffusion of the target molecules into the pore channels and makes the internal surface areas available for photocatalytic reaction, thus contributing to the high activity.

Acknowledgment

We thank National Science Council (Contract Nos. NSC 100-2627-M-009-001 and NSC 101-3113-E-009-003) for financially supporting this research.

References

[1] S.M. Chang, P.H. Lo, C.T. Chang, Applied Catalysis B: Environmental 91 (2009) 619–627.
[2] S.M. Chang, C.Y. Hou, P.H. Lo, C.T. Chang, Applied Catalysis B: Environmental 90 (2009) 233–241.
[3] G.J.D.A. Soler-Illia, A. Louis, C. Sanchez, Chemistry of Materials 14 (2002) 750–759.
[4] J. Hwang, J. Kim, E. Ramasamy, W. Choi, J. Lee, Microporous and Mesoporous Materials 143 (2011) 149–156.
[5] Z. Ma, J.H. Yu, S. Dai, Advanced Materials 22 (2010) 261–285.
[6] J. Zhang, Q.H. Zhang, X.L. Li, S.M. Liu, Y.B. Ma, F. Shi, Y.Q. Deng, Physical Chemistry Chemical Physics 12 (2010) 1971–1981.
[7] E.R. Cooper, C.D. Andrews, P.S. Wheatley, P.B. Webb, P. Wormald, R.E. Morris, Nature 430 (2004) 1012–1016.
[8] Y. Zhou, J.H. Schattka, M. Antonietti, Nano Letters 4 (2004) 477–481.
[9] S. Dai, Y.H. Ju, H.J. Gao, J.S. Lin, S.J. Pennycook, C.E. Barnes, Chemical Communications (2000) 243–244.
[10] Y. Zhou, M. Antonietti, Journal of the American Chemical Society 125 (2003) 14960–14961.
[11] K.S. Yoo, T.G. Lee, J. Kim, Microporous and Mesoporous Materials 84 (2005) 211–217.
[12] H. Choi, Y.J. Kim, R.S. Varma, D.D. Dionysiou, Chemistry of Materials 18 (2006) 5377–5384.
[13] C.C. Han, S.Y. Ho, Y.P. Lin, Y.C. Lai, W.C. Liang, Y.W. Chen-Yang, Microporous and Mesoporous Materials 131 (2010) 217–223.
[14] Y. Shiraishi, N. Saito, T. Hirai, Journal of the American Chemical Society 127 (2005) 12820–12822.
[15] K. Yang, Y. Sun, Biochemical Engineering Journal 37 (2007) 298–310.
[16] T.K. Yun, S.S. Park, D. Kim, Y.K. Hwang, S. Huh, J.Y. Bae, Y.S. Won, Journal of Power Sources 196 (2011) 3678–3682.
[17] R.S. Yuan, R.B. Guan, J.T. Zheng, Scripta Materialia 52 (2005) 1329–1334.
[18] J. Du, X.Y. Lai, N.L. Yang, J. Zhai, D. Kisailus, F.B. Su, D. Wang, L. Jiang, ACS Nano 5 (2011) 590–596.
[19] S. Lacombe, H. Cardy, N. Soggiu, S. Blanc, J.L. Habib-Jiwan, J.P. Soumillion, Microporous and Mesoporous Materials 46 (2001) 311–325.
[20] A. Shimojima, M. Sakurai, K. Kuroda, T. Okubo, Journal of Colloid and Interface Science 350 (2010) 155–160.
[21] Y.H. Deng, J. Liu, C. Liu, D. Gu, Z.K. Sun, J. Wei, J.Y. Zhang, L.J. Zhang, B. Tu, D.Y. Zhao, Chemistry of Materials 20 (2008) 7281–7286.
[22] J. Hu, F. Gao, Y.Z. Shang, C.J. Peng, H.L. Liu, Y. Hu, Microporous and Mesoporous Materials 142 (2011) 268–275.
[23] L. Pauling, Nature of the Chemical Bond, 2nd ed., Cornell University Press, Ithaca, N.Y., 1948.
[24] S. Kaciulis, G. Mattogno, L. Pandolfi, M. Cavalli, G. Gnappi, A. Montenero, Applied Surface Science 151 (1999) 1–5.
[25] M.T. Rinke, L. Zhang, H. Eckert, Chemphyschem 8 (2007) 1988–1998.

[26] V. Simon, D. Muresan, A.F. Takacs, M. Neumann, S. Simon, Solid State Ionics 178 (2007) 221–225.
[27] K.R. Reyes-Gil, E.A. Reyes-Garcia, D. Raftery, Journal of Physical Chemistry C 111 (2007) 14579–14588.
[28] H.Q. Sun, Y. Bai, H.J. Liu, W.Q. Jin, N.P. Xu, G.J. Chen, B.Q. Xu, Journal of Physical Chemistry C 112 (2008) 13304–13309.
[29] D.L. Tian, X.F. Zhang, J. Zhai, L. Jiang, Langmuir 27 (2011) 4265–4270.
[30] S.G. Zhang, M. Ariyuki, H. Mishima, S. Higashimoto, H. Yamashita, M. Anpo, Microporous and Mesoporous Materials 21 (1998) 621–627.
[31] K.O. Agenson, J.I. Oh, T. Urase, Journal of Membrane Science 225 (2003) 91–103.
[32] G.K. Ackers, Molecular-Sieve Processes 3 (1964) 723–730.